

Muon detection in electron-positron annihilation for muon collider studies

N. Amapane^{a,b}, M. Antonelli^c, F. Anulli^d, G. Ballerini^{e,f}, L. Bandiera^g, N. Bartosik^b, M. Bauce^d, A. Bertolin^h, C. Biino^b, O. R. Blanco-Garcia^c, M. Boscolo^c, C. Brizzolari^{e,f}, A. Cappati^{a,b}, F. Casaburo^{i,d,*}, M. Casarsa^j, G. Cavoto^{i,d}, G. Cesarini^{i,d}, F. Collamati^d, G. Cotto^{a,b}, C. Curatolo^h, R. Di Nardo^k, F. Gonella^h, S. Hoh^{l,h}, M. Iafrati^c, F. Iacoangeli^d, B. Kiani^b, R. Li Votiⁱ, D. Lucchesi^{k,h}, V. Mascagna^{e,f}, A. Paccagnella^{k,h}, N. Pastrone^b, J. Pazzini^{k,h}, M. Pelliccioni^{a,b}, B. Ponzio^c, M. Prest^{e,f}, M. Ricci^c, S. Rosati^d, R. Rossin^{l,h}, M. Rotondo^c, O. Sans Planell^{a,b}, L. Sestini^h, M. Soldani^{e,f}, A. Triossi^m, E. Vallazza^f, S. Ventura^h, M. Zanetti^{l,h}

^aUniversità degli Studi di Torino- Torino, Italy

^bINFN Sezione Torino- Torino, Italy

^cINFN Laboratori Nazionali di Frascati - Frascati, Italy

^dINFN Sezione Roma- Rome, Italy

^eUniversità degli Studi dell'Insubria - Como, Italy

^fINFN Sezione di Milano Bicocca - Milan, Italy

^gINFN Sezione di Ferrara - Ferrara, Italy

^hINFN Sezione di Padova - Padova, Italy

ⁱSapienza Università di Roma- Roma, Italy

^jINFN Sezione di Trieste - Trieste, Italy

^kCERN - Geneva, Switzerland

^lUniversità di Padova - Padova, Italy

^mInstitut Pluridisciplinaire Hubert Curien, Strasbourg, France

Abstract

The investigation of the energy frontier in physics requires novel concept for future colliders. The idea of a muon collider is very appealing since it would aim to study particle collisions up to tens of TeV energy while offering a cleaner experimental environment with respect to hadronic colliders. One key element in the muon collider design is muon production with small emittance. Recently, the Low EMittance Muon Accelerator (LEMMA) collaboration has explored the close-to-threshold muon production by 45 GeV positron annihilating in a low Z material target. Muons are emerging with a natural small emittance. In this

*Corresponding author

Email address: fausto.casaburo@uniroma1.it (F. Casaburo)

paper we describe the performance of a system of segmented absorbers with alternating active layers realized with fast Cherenkov detectors and a muon identification technique based on it. Passive layers were made of tungsten. Muons and electron beams data were collected in September 2018 at the H2 line in the North Area of the Conseil Européen pour la Recherche Nucléaire (CERN).

Keywords: Muon Collider, Cherenkov detectors

Contents

Introduction	2
1 Experimental Setup	4
2 Absorbers system performance studies	10
2.1 Data acquisition	10
2.2 Tracker - absorbers correlation	11
2.3 Lead Glass (LG) calibration	12
2.4 HORSА efficiency	13
2.5 HORSА electron contamination	14
2.6 HORSА Muon detection	15
3 Particles detection in positron beam data with target	16
3.1 Data to Monte Carlo (MC) simulations comparisons	18
Conclusions	19
Acknowledgements	20

Introduction

Exploring the high energy frontier represents a great opportunity to investigate the fundamental laws of nature. This requires a future particle collider able to accelerate elementary particles to the highest possible energy. A muon

collider represents an appealing though challenging solution for this [1, 2]. Previous studies proposed that a muon collider is conceivable to explore the multi-TeV energy frontier with the possibility to study Higgs boson properties [2]. Muons are in fact emitting much less radiation than electrons with the same energy, then a muon collider can reach a Center of Mass (CM) energy higher than an electron one; however the $2.2\ \mu\text{s}$ muon lifetime is posing hard constraints on the design of the accelerator complex. For instance, small emittance is one of the critical elements towards a high luminosity muon collider.

The LEMMA project aims to study the possibility of producing muons from the e^+e^- annihilation process. A high intensity positron beam, with an energy just above the 43.7 GeV production threshold, impinging on a low Z fixed target could produce muons with small divergence, resulting in a small transverse emittance [3]. This would avoid the need of beam cooling, otherwise required in a production scheme based on pion decays as pursued in the Muon Accelerator Program (MAP) [4]. Experimental data in this specific energy regime are not frequent as most of the measurements are performed at higher \sqrt{s} values [5]. It is therefore necessary to measure the cross section and the $\mu^+\mu^-$ kinematic properties for several values of the center of mass energy near the threshold to probe such predictions.

While the leading-order Quantum ElectroDynamics (QED) $e^+e^- \rightarrow \mu^+\mu^-$ cross-section calculations are well established, at threshold higher order radiative effects, due to Coulomb interaction, might be important to predict the muons production rate and their angular distribution [6]. A dedicated experimental effort has been put in place to study muon production by 45 GeV positrons impinging in beryllium or carbon targets [7].

The aim of this paper is to describe a system of segmented and instrumented absorbers, named HORSAs (Fig. 1) and VERSAs in the following, that can be used to effectively study the $e^+e^- \rightarrow \mu^+\mu^-$ process near the threshold region.

These absorbers were part of the apparatus deployed at the CERN North Area beam lines during the 2017 and 2018 data-taking periods. They were meant to identify both positive and negative muons against electrons and positrons.

They were initially conceived as massive but portable devices that could be employed as sampling calorimeters to study the hadronic shower development initiated by the Large Hadron Collider (LHC) beam interactions [8]. Their performance in terms of muon identification have been tested using electron and muon beams. Results regarding of the performances of the HORSa absorber are described in Section 2. In addition, to test these performances, the observed ratio of the number of muons to electrons events in 45 GeV positron beam data hitting on carbon targets is reported and compared with a Monte Carlo (MC) simulation in Section 3.

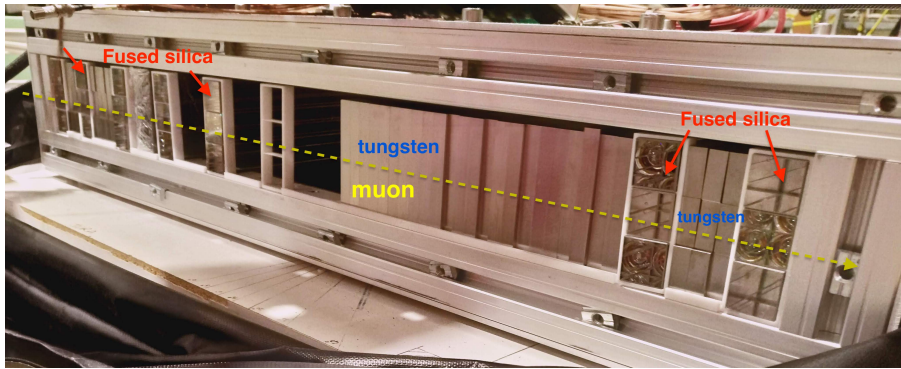


Figure 1: HORSa absorber during its assembly phase. Fused silica bars are alternated with tungsten bricks.

1. Experimental Setup

The experimental setup consists of a ~ 23 m long apparatus showed in Fig. 2 (vacuum pipe, target and magnetic spectrometer region) and Fig. 3 (absorbers region) that was installed at the H2 beam line of the CERN North Area in summer 2018, to measure with high precision trajectories and momenta of the two final state muons as well as the direction of the incoming positrons.

Upstream of the fixed target (Fig. 2), primary positrons are crossing a pair of $2 \times 2 \text{ cm}^2$ silicon sensors, constituted by two layers of orthogonal microstrips in order to measure the incoming particle direction and position. Always upstream, a scintillator was used for trigger purposes.

Downstream of the target (Fig. 2), all secondary particles emerging cross another silicon sensor pair in order to measure their direction before entering a dipole magnet (with a 2.01 T field along y , extended in a region of approximately ± 1000 cm along z).

The secondary particles (either e^+e^- or $\mu^+\mu^-$) are individually reconstructed and their momentum is determined by measuring their deflection in the x - z plane with a two arms silicon sensor system located downstream of the magnet (Fig. 2).

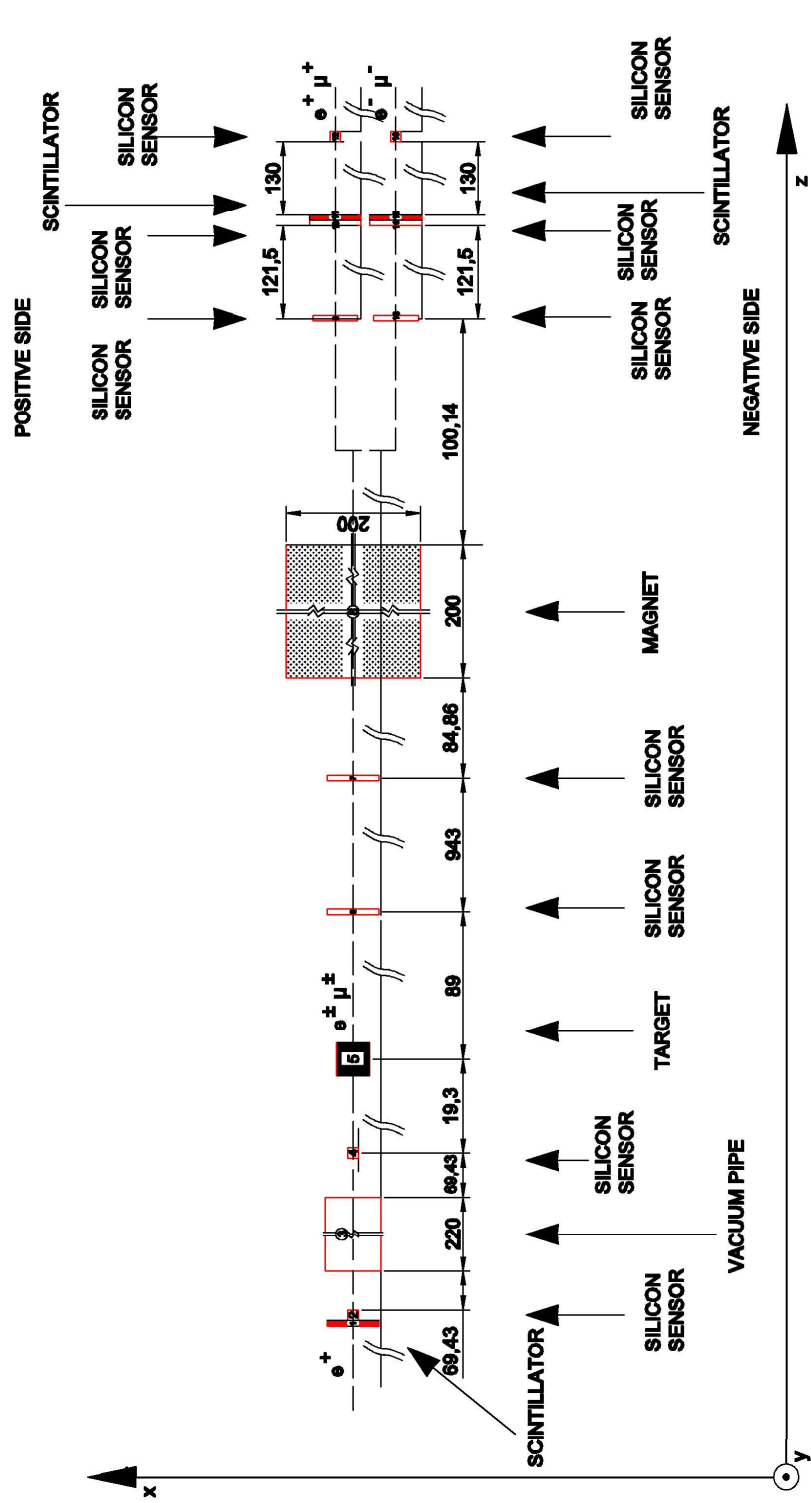


Figure 2: Magnetic spectrometer setup installed at the H2 beam line of CERN to study the particles emerging from a low Z target in positron annihilation processes.

Particles are then entering the absorbers region (Fig. 3) where the detectors are also organized in two arms. Each arm is constituted by two trigger scintillators and the massive absorbers. An iron block is also employed to shield Drift Tube (DT) muon chambers located further downstream (not displayed in Fig. 3).

Each active absorber is made of a three unit Lead Glass (LG) electromagnetic calorimeter, each unit featuring a 40 cm deep truncated pyramid shape. The instrumented absorber is installed immediately after the LG calorimeter.

The absorber named HORSa is installed in the arm where the negative particles (either e^- or μ^-) are deflected by the magnetic field. It is equipped with 1 inch thick fused silica layers where secondary charged particles are producing Cherenkov light. Three photomultiplier (PMT) are used to detect the light produced in each of the fused silica layers and transmitted to the PMTs by internal reflection along the x direction, i.e. the direction transverse to the beam (Fig. 2). A sequence of alternating active and passive layers along z are used to filter muons against electrons. Among the first (second) pair of fused silica layers a 5 cm (3 cm) tungsten shield is inserted. Among the two fused silica layer pairs of 23 cm thick tungsten elements are also inserted. Other fused silica and graphite layers are present. These however are not readout and not massive enough to be relevant for electron/muon discrimination.

A second instrumented absorber, named VERSa, with a different internal segmentation, is installed on the arm where the main positron beam and the positively charged secondaries are deflected. Its performances are not described in this paper.

Two typologies of triggers were used for the shared silicon sensors and calorimeters Data Acquisition System (DAQ): a first one (named *single*) based on the signals produced by the scintillator placed upstream of the target (Fig. 2) and a second one (named *muon*) based on this upstream scintillator signal in coincidence with the signals of additional scintillators (four in total) positioned, respectively, upstream of the LG blocks and downstream of the muon chambers (Fig. 3), on the two arms of the detector. The *single* trigger was used to se-

lect events with no bias on the final state while the *muon* trigger was used to enhance the content of $\mu^+\mu^-$ events in the data sample.

The DT chambers were using an independent trigger-less DAQ system, with an acquisition rate of 40 MHz. The trigger signal from the scintillators was shared between the two DAQ systems for offline synchronisation and event building.

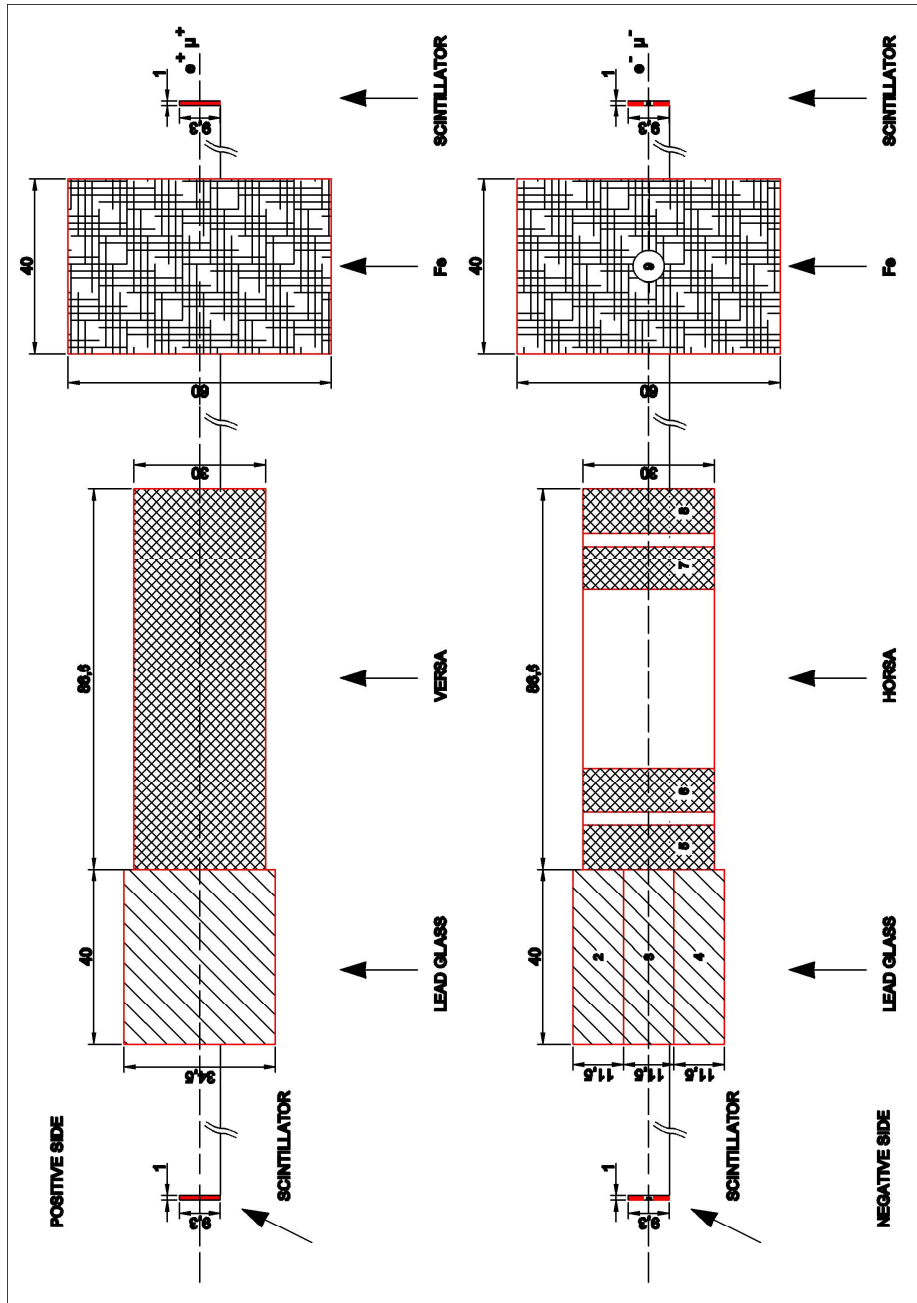


Figure 3: Absorber region installed downstream the magnetic spectrometer.

2. Absorbers system performance studies

2.1. Data acquisition

Beam data were recorded during the summer 2018 data-taking campaign. Electron and muon beams of different energies, without the target in position and a 45 GeV positron beam hitting the target were delivered to the experimental region. In particular muon beams with energy set to $E^* = 22$ GeV, without target, and with both magnetic field directions have been used for the alignment of the silicon detectors and the muon chambers.

Muon and electron beams, both with energy E^* and no target inserted are also used to estimate the detectors performances. Indeed, the energy E^* is approximately equal to the mean energy of the muons produced in the $e^+e^- \rightarrow \mu^+\mu^-$ process when initiated by a 45 GeV positron beam. The magnet is operated to deflect particles with this energy into the downstream double-arm section: particles with energy E^* are in fact hitting the central unit of the LG calorimeter. In addition, to study muon production close to threshold, a 45 GeV positron beam was delivered to some targets installed in different data-taking runs. In this analysis, two carbon targets with 2 cm and 6 cm thickness and a diameter of 4 cm have been used (sec. 3). The positron beam had a pulsed shape with 4 spills per minute, each spill lasting 4.8 s with a typical intensity of $5 \cdot 10^6$ positrons. The spot size was $\sim 2 \times 2$ cm² with an angular spread of ~ 300 μ rad. With the chosen collimators setting the momentum spread was below 1.5 % [9] and the purity of the beam was in the range 95 – 99 % [10].

Data were acquired including information about the arrival times, the released energy in each constituent of the absorbers and the particle positions detected by the silicon trackers. Both *muon* and *single* triggers (with a prescaling factor of about $3 \cdot 10^4$) were enabled in the acquisition with the 45 GeV positron beam hitting the target.

Events with the final state $\mu^+\mu^-$ or e^+e^- were identified by using the LG and the HORSa absorber located on the negative side, i.e. only identifying the negative particle in the final state. The $\mu^+\mu^-$ events are mainly due to

the e^+e^- annihilation process while the e^+e^- final state is produced in e^+e^- Bhabha scattering of the positron beam with a target atomic electron or in pair production by a high energy photon in the target [11].

Electrons with energy E^* are producing an electromagnetic shower that is almost entirely contained in the LG central unit. Negative muons, on the contrary, are crossing the LG and HORSAs detectors producing a signal in the LG central unit and in all the HORSAs active layers. Exploiting this different behaviour, the ratio of the number of observed events with a muon or an electron, μ^-/e^- , can then be computed. With an estimate of the efficiency to detect muons and electrons with energy E^* the $\mu^+\mu^-/e^+e^-$ ratio, for events reaching the absorber region, can then be inferred. This ratio can eventually be compared with a MC simulation of the experimental layout.

The Cherenkov light produced in the LG and HORSAs active elements is readout by PMTs Hamamatsu R7378A [12]. The LG PMT signals were digitized by a 12 bit @250 MS/s Flash ADC Waveform Digitizer CAEN V1720 [13] while the HORSAs PMT by a 14 bit @500 MS/s Flash ADC Waveform Digitizer CAEN V1730 [14]. Information about the time and the charge associated with these signals were stored for the off-line analysis.

A 22 GeV muon is releasing only a fraction of its energy in the absorber materials and it is therefore not stopped by them. Moreover, only a fraction of the energy loss is deposited as Cherenkov light and eventually detected by the PMTs. A 22 GeV muon event candidate is defined by the time coincidence of the PMT signals from all the five trigger scintillators, the central LG unit and the four HORSAs active layers, with the requirement to be in anti-coincidence with the two external LG units.

2.2. Tracker - absorbers correlation

As previously anticipated, the magnet deflects 22 GeV particles towards the central unit of the LG (block 3 in Fig. 3). Therefore, the first step of this analysis has been to get a relation between the x position of particles crossing the tracker (Fig. 2) positioned just before the first scintillator of the negative

arm and the energy released in the central LG unit. Fig. 4 shows the average released energy in the central LG unit by 22 GeV electrons (blue) and 22 GeV muons (green) as a function of the x position of these particles recorded by the tracker.

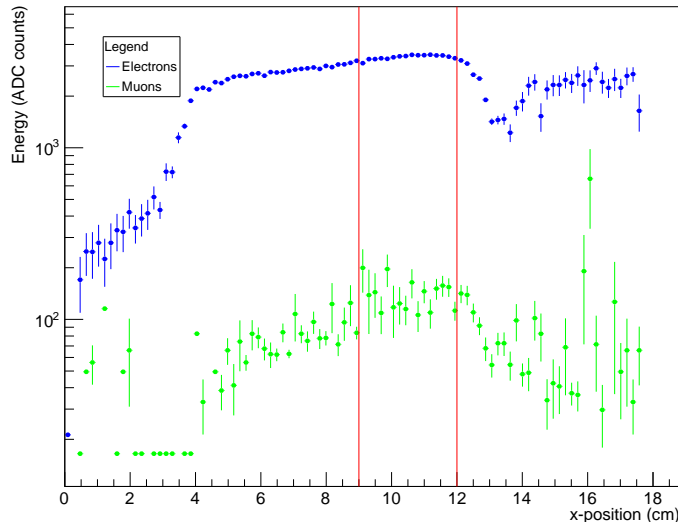


Figure 4: Average released energy by 22 GeV electrons (blue) and muons (green) in central LG as a function of the position recorded by the tracker. Vertical red lines are used to mark the region $9 \text{ cm} < x < 12 \text{ cm}$ in the graph.

The largest released energy occurs for particles with tracker coordinates in the range $9 \text{ cm} < x < 12 \text{ cm}$, both for muons and electrons. This requirement is therefore retained for the subsequent studies.

2.3. Lead Glass (LG) calibration

22 GeV electron beam data with no target has been used to study the released energy in the central unit of the LG. Events in time coincidence between the scintillator (Fig. 3) and the three LG units were employed. The spectrum of released energy in the central LG unit is shown in Fig. 5 and interpolated with a Gaussian.

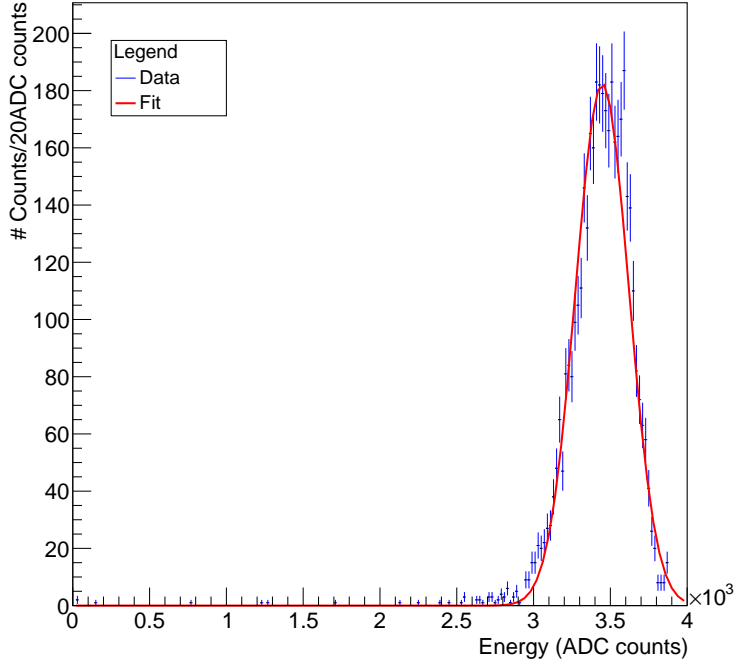


Figure 5: Energy calibration of the LG with a 22 GeV electron beam.

The mean value and the square root of the variance, as returned by the fit, are $\mu = 3447$ ADC and $\sigma = 174$ ADC, respectively. Given that electrons are expected to release all energy in the LG block, the calibration $1 \text{ GeV} = (156.7 \pm 7.9)$ ADC counts is then obtained. The quoted uncertainty is statistical only, systematic effects are believed to be negligible compared to it and to have a small impact for the studies presented later on.

In later sections, in order to define a candidate muon event, the requirement on the released energy E_3 (subscript number refers to Fig. 3) in the central LG unit $E_3 < 1 \text{ GeV}$ is used.

2.4. HORSА efficiency

The efficiency of each HORSА active layer has been studied using the 22 GeV muon beam. Defining $N_4(j)$ and $N_3(j)$ the numbers of events in time coincidence

in the four or three HORSAs layers (excluding the j^{th} layer), respectively, we define the efficiency of the $j = 5, 6, 7, 8$ layers (numbers refer to Fig. 3) as:

$$\varepsilon_j = \frac{N_4(j)}{N_3(j)} \quad (1)$$

The overall efficiency of the HORSAs absorber is given by

$$\varepsilon_{HORSAs} = \prod_{j=5}^8 \varepsilon_j \quad (2)$$

Results as obtained from the 22 GeV muon beam data, with the statistical uncertainties computed applying the Gaussian statistics (i.e. the uncertainty on N events is $\sigma = \sqrt{N}$), are given in Tab. 1.

Table 1: Efficiencies to detect a 22 GeV muon in each of the fused silica HORSAs layers and overall HORSAs efficiency.

j	ε_j	ε_{HORSAs}
5	$(9.70 \pm 0.39) \cdot 10^{-1}$	$(8.42 \pm 0.80) \cdot 10^{-1}$
6	$(9.55 \pm 0.38) \cdot 10^{-1}$	
7	$(9.33 \pm 0.46) \cdot 10^{-1}$	
8	$(9.75 \pm 0.55) \cdot 10^{-1}$	

2.5. HORSAs electron contamination

To estimate the electron contamination in the HORSAs absorber, a 22 GeV electron beam is used. The HORSAs contamination is given by:

$$c_{HORSAs} = \frac{N_{HORSAs}}{N_{Tot}} \quad (3)$$

where N_{HORSAs} is the number of events in time coincidence in the four HORSAs layers and N_{Tot} is the total number of acquired events. Applying the Feldman-Cousins (FC) method, the Upper Limit (UL) on this ratio is $2 \cdot 10^{-4}$ at 90% CL , being $N_{HORSAs} = 1$ and $N_{Tot} = 21504$.

2.6. HORSА Muon detection

Muons, while are crossing the LG and HORSА detectors, produce a signal in the LG central unit and in all the HORSА active layers.

The total observable energy released in the central LG unit and in the HORSА absorber is:

$$E_{obs} = E_3 + E_{HORSА}. \quad (4)$$

where E_3 (subscript number refers to Fig. 3) is the released energy in the central unit of the LG (Fig. 6) and $E_{HORSА} = \sum_{j=5}^8 E_j$ (subscript numbers refer to Fig. 3).

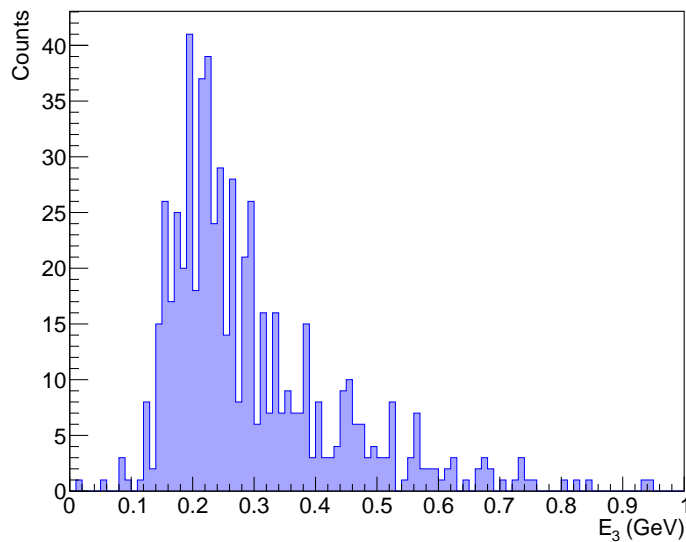


Figure 6: Released energy in LG central unit by a 22 GeV muon beam data sample.

The correlation between E_3 and $E_{HORSА}$ (Fig. 7) shows that the total energy released by 22 GeV muons in HORSА is $E_{HORSА} < 2000$ ADC. This condition can be therefore used to define a signal region to select muons produced in the 45 GeV e^+ beam data with target.

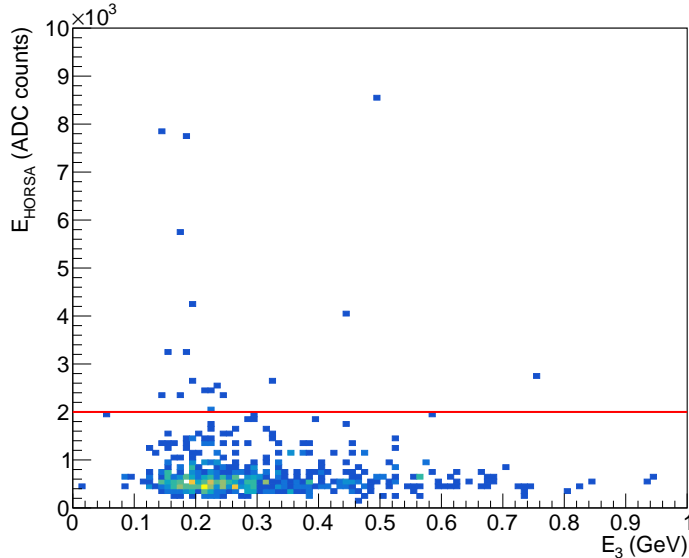


Figure 7: Released energy in HORSA in function of released energy in the LG central unit by a 22 GeV muon beam data sample. Red line is used to mark the signal region.

3. Particles detection in positron beam data with target

To test the detector performance, the μ^-/e^- events ratio was calculated by estimating the yield of 22 GeV μ^- and 22 GeV e^- events produced by the positron beam impinging on different targets.

With reference to Fig. 3, candidate muon events have been selected requiring the coincidence in time between the two trigger scintillators (the first one upstream of the LG block and the second one downstream of the muon chamber), the LG central unit and all the HORSA layers; anti-coincidence with the LG external units (numbered 2 and 4 in Fig. 3) is required as well. To suppress the background in the signal region $E_{HORSA} < 2000$ ADC, the sideband-subtraction method has been applied: assuming an uniform background distribution in and out of the signal region, the muons yield after the sideband-subtraction is given by:

$$N_{\mu_{det}^-} = N_{\mu^-} - \alpha N_{side} \quad (5)$$

where N_{μ^-} and N_{side} are respectively the number of candidate muon events in the signal and the number of background events in the sideband regions.

The α parameter has been estimated as $\alpha = \frac{2000 \text{ ADC}}{E_{max} - 2000 \text{ ADC}}$, where E_{max} is the maximum energy of the sideband region (the targets have an average maximum energy $E_{max} \sim 30000 \text{ ADC}$).

With reference to Fig. 3, an electron from the e^+e^- final state is selected requiring the time coincidence between the two trigger scintillators (one for each arm of the detector) positioned upstream of the LG blocks and the central unit of the LG in the negative arm. The time anti-coincidence with the two trigger scintillators (one for each arm of the detector) positioned downstream to the muon chambers is also required.

Defining $N_{e_{det}^-}$ and ε_{e^-} respectively the number of detected electrons and the efficiency to detect them and using the result for the muon detection efficiency $\varepsilon_{HORS A}$ (Tab. 1), the ratio between produced muons and electrons is:

$$N_{\mu^-}/N_{e^-} = \frac{N_{\mu_{det}^-}/\varepsilon_{HORS A}}{N_{e_{det}^-}/\varepsilon_{e^-}} \quad (6)$$

Lastly, given that the efficiency to detect an electron is close to unity, the overall efficiency ratio can be assumed to be $\varepsilon \sim \varepsilon_{HORS A}$ and $N_{e_{det}^-} \sim N_{e^-}$; therefore Eq. 6 can be rewritten as:

$$N_{\mu^-}/N_{e^-} = \frac{N_{\mu_{det}^-}/N_{e^-}}{\varepsilon} \quad (7)$$

The results regarding the μ^-/e^- ratios on the different targets exposed to the beam are summarized in Tab. 2. The uncertainties indicated have been calculated by applying Gauss statistic when the number of counts was larger than 30 or Poisson statistic otherwise. Several source of systematic uncertainties have been taken into account. The majority of the conceivable effects will have the same impact on the electron and muon detection. Hence, at fist order, they will cancel in the ratio. Moreover the limited statistic available in the muon sample was also an obstacle for further investigations on systematic effects.

Table 2: N_{μ^-}/N_{e^-} ratio for carbon targets.

Thickness (cm)	N_{e^-}	$N_{\mu_{det}^-}$	N_{μ^-}/N_{e^-}
2	85.0 ± 9.2	37.0 ± 6.6	$(5.1 \pm 1.2) \cdot 10^{-1}$
6	78.0 ± 8.8	$5.0_{-3.0}^{+4.1}$	$(7.6_{-4.6}^{+6.4}) \cdot 10^{-2}$

3.1. Data to Monte Carlo (MC) simulations comparisons

In order to test the particle detection ability of the absorbers system showed previously (Tab. 2), Geant4 [15, 16] based MC simulations of the standard electromagnetic interactions of particles with matter, have been performed to compare the μ^-/e^- events ratio obtained in data with theoretical predictions. As far as primary particles are concerned, several options have been implemented besides the possibility to simulate a 45 GeV positron beam along the z -axis, with characteristics equivalent to the experimental ones.

Samples of 10^8 45 GeV primary e^+ hitting carbon (both 2 cm and 6 cm thickness) targets have been simulated in order to estimate the number $N_{e_{MC}^-}$ of produced e^- .

Due to the low cross section of muon production in the annihilation process, simulations regarding the number $N_{\mu_{MC}^-}$ of produced μ^- , were made by generating samples of 10^7 45 GeV primary e^+ and by setting a bias (i.e. a technique to enhance any electromagnetic cross section by a defined factor) equal to 1000 for the $e^+e^- \rightarrow \mu^+\mu^-$ cross section [17]. Then the obtained number of produced muons refers to a total of 10^{10} primary positrons. This allowed the simulation of enough $e^+e^- \rightarrow \mu^+\mu^-$ events in a reasonable time.

The obtained results, with their statistical uncertainties (computed applying the Gaussian statistics), are given in Tab. 3 in which the number of produced electrons has been normalized to 10^{10} primary positrons.

Table 3: μ^-/e^- MC based ratios for carbon targets. The numbers of e^- have been normalized to 10^{10} primary e^+ .

Thickness (cm)	$N_{e_{MC}^-}$	$N_{\mu_{MC}^-}$	$N_{\mu_{MC}^-}/N_{e_{MC}^-}$
2	2400 ± 49	1481 ± 38	$(6.2 \pm 1.3) \cdot 10^{-1}$
6	$(521 \pm 2.3) \cdot 10^2$	2870 ± 54	$(5.51 \pm 0.26) \cdot 10^{-2}$

The experimental results (Tab. 2) are well compatible, within uncertainties, with the MC prediction (Tab. 3).

Conclusions

The implementation of the LEMMA muon collider concept needs a intense positron beam to produce enough muons. The knowledge of the muon production cross section close to threshold is extremely important for the design of a muon collider.

In this paper we reported the results of a muon identification technique based on segmented massive absorbers that can be used in experiments to measure the properties of the muons produced by the e^+e^- annihilation process at threshold. Several unexpected difficulties during the acquisition campaigns has led to a yield of just few tens of electron and muon events produced. However these events allowed to test the performance of the described absorbers system. These data also allowed a comparison with MC simulation, showing an agreement between experimental data and MC. Therefore this system and this method can be used for future studies of the $e^+e^- \rightarrow \mu^+\mu^-$ process at the threshold energy.

Several accelerator technologies studies, like the development of a muon collider with the LEMMA injection scheme, could benefit from these measurements.

In order to increase statistics and reduce backgrounds, i.e. to provide a meticulous measurement of $e^+e^- \rightarrow \mu^+\mu^-$ cross section, more accurate tracking devices, alignment infrastructures and a more efficient trigger and readout

systems will be needed. An upgrade of the LEMMA experimental layout is foreseen in order to accumulate more data at the threshold energy.

With an adequately low energy spread and with a larger beam rate this apparatus might also be employed to search for bound states as the true muonium [18].

Acknowledgements

We would like to warmly thanks the Super Proton Synchrotron (SPS) staff and the Large Scale Metrology (LSM) group, in particular Henrik Wilkens and Nikolaos Charitonidis, for their support during installation and data taking. This work has been supported by the ERC CoG GA 615089 CRYSBEAM.

References

- [1] R. Franceschini, M. Greco, Higgs and bsm physics at the future muon collider (2021). [arXiv:2104.05770](https://arxiv.org/abs/2104.05770).
- [2] The Muon Accelerator Program, <https://map.fnal.gov/>.
- [3] M. Antonelli, M. Boscolo, R. Di Nardo, P. Raimondi, Novel proposal for a low emittance muon beam using positron beam on target (2016). [arXiv:1509.04454](https://arxiv.org/abs/1509.04454), [doi:10.1016/j.nima.2015.10.097](https://doi.org/10.1016/j.nima.2015.10.097).
- [4] N. Palmer, et al., Proceedings of the 1996 DPF/DPB Summer Study on High-Energy Physics, in: Stanford Linear Accelerator Center, Menlo Park, CA , 1997.
- [5] M. Thomson, Modern Particle Physics, Cambridge University Press, 2013. [doi:10.1017/CB09781139525367](https://doi.org/10.1017/CB09781139525367).
- [6] Y. M. Bystritskiy, E. A. Kuraev, G. V. Fedotov, F. V. Ignatov, [Cross sections of muon and charged pion pair production in electron-positron annihilation near the threshold](https://arxiv.org/abs/hep-th/0502154), Phys. Rev. D 72 (2005) 114019. [doi:](https://doi.org/10.1103/PhysRevD.72.114019)

[10.1103/PhysRevD.72.114019](https://doi.org/10.1103/PhysRevD.72.114019).

URL <https://link.aps.org/doi/10.1103/PhysRevD.72.114019>

- [7] N. Amapane, et al., Study of muon pair production from positron annihilation at threshold energy, JINST 15 (01) (2020) P01036. [arXiv:1909.13716](https://arxiv.org/abs/1909.13716), [doi:10.1088/1748-0221/15/01/P01036](https://doi.org/10.1088/1748-0221/15/01/P01036).
- [8] F. Iacoangeli, F. Addesa, L. Bandiera, E. Bagli, G. Cavoto., An instrumented absorber detector for hadronic interaction measurements : (The Smart Absorber of Crysbeam project), in: 2018 IEEE Nuclear Science Symposium and Medical Imaging Conference, 2018, p. 8824636. [doi:10.1109/NSSMIC.2018.8824636](https://doi.org/10.1109/NSSMIC.2018.8824636).
- [9] G. Brianti, et al., SPS North Experimental Area 2013 General Layout, CERN/LAB II/EA/Note (73-4) (1973).
- [10] N. Charitonidis, Private Communication (2018).
- [11] F. Mandl and G. Shaw, Quantum Field Theory, John Wiley & Sons, 1984.
- [12] Hamamatsu, https://www.hamamatsu.com/resources/pdf/etd/R7378A_TPMH1288E.pdf.
- [13] CAEN Tools for Discovery, <https://www.caen.it/products/v1720/>.
- [14] CAEN Tools for Discovery, <https://www.caen.it/products/v1730/>.
- [15] Geant4 Community, <https://geant4.web.cern.ch/node/1>.
- [16] S. Agostinelli, et al., GEANT4: A simulation toolkit, Nucl. Instrum. Meth. A506 (2003) 250–303. [doi:10.1016/S0168-9002\(03\)01368-8](https://doi.org/10.1016/S0168-9002(03)01368-8).
- [17] J. Allison, J. Apostolakis, A. Bagulya, C. Champion, S. Elles, F. Garay, V. Grichine, A. Howard, S. Incerti, V. Ivanchenko, J. Jacquemier, M. Maire, A. Mantero, P. Nieminen, L. Pandola, G. Santin, D. Sawkey, A. Schälicke, L. Urban, [Geant4 electromagnetic physics for high statistic simulation of LHC experiments](#), Journal of Physics: Conference Series 396 (2) (2012)

022013. [doi:10.1088/1742-6596/396/2/022013](https://doi.org/10.1088/1742-6596/396/2/022013).

URL <https://doi.org/10.1088/1742-6596/396/2/022013>

- [18] S. J. Brodsky, R. F. Lebed, Production of the Smallest QED Atom: True Muonium ($\mu^+ \mu^-$), Phys. Rev. Lett. 102 (2009) 213401. [arXiv:0904.2225](https://arxiv.org/abs/0904.2225), [doi:10.1103/PhysRevLett.102.213401](https://doi.org/10.1103/PhysRevLett.102.213401).